J|A|C|S
ARTICLES
Published on Web 06/27/2006

Self-Assembly of Organic Monolayers on Aerosolized Silicon Nanoparticles

Ying-Chih Liao and Jeffrey T. Roberts*

Contribution from the Department of Chemistry, University of Minnesota, 207 Pleasant Street SE, Minneapolis, Minnesota 55455

Received February 16, 2006; E-mail: liao@chem.umn.edu; roberts@chem.umn.edu

Abstract: A new method is described for surface functionalization of silicon nanocrystals. Organic monolayers were self-assembled via gas-phase adsorption of amines, alkenes, alkynes, and aldehydes onto the surfaces of aerosolized crystalline silicon nanoparticles of 12.2 nm diameter in an atmospheric pressure tube reactor. Assembly took place within 4 s at temperatures between 200 and 500 °C. The extent of adsorption was measured by using tandem differential mobility analysis (T-DMA), an on-line diagnostic method for measuring changes in particle size. Functionalized particles were further characterized by high-resolution transmission electron microscopy and diffuse reflectance Fourier transform infrared spectroscopy. The apparatus described in this work can be used for continuous mass production of functionalized silicon nanoparticles. Moreover, the overall strategy of using T-DMA for monitoring monolayer uptake could be generally applied to study surface processing of other aerosolized nanoparticle systems.

Introduction

Silicon nanoparticles have many potential device applications, including LEDs,[1,2] bioprobes,[3] semiconductors,[4] and solar cells.[5] Many preparation methods for silicon nanocrystals have been described in the literature, such as silicon wafer anodization,[6] oxidation of silicides, reduction of silicon halides,[7] laser ablation,[8] and nonthermal plasma synthesis.[9] Silicon nanoparticles are susceptible to rapid ambient air oxidation, which results in degradation of optical and electrical properties.[10] Surface protection or passivation therefore is essential for high-added value applications involving silicon nanoparticles. Surface layers can also help prevent coagulation. Moreover, the functional groups on the surface layer can help direct particle adsorption to specific sites on a substrate, and thus enable certain device applications. Among various surface passivation methods for silicon nanoparticles, attachment of organic molecules to particle surfaces, for instance by hydrosilylation chemistry, is considered a promising approach because of the well-insulated layer and selective surface functional groups for further usage. Previously reported hydrosilylation processes are usually performed batchwise in an organic solvent and require reaction times of hours, as well as thermal activation or photocatalysis.[11−14] For large production rates, it would be preferable to produce functionalized particles continuously. Among the available silicon nanoparticle syntheses, gas-to-particle conversion methods provide a fast, reliable, and continuous particle source. A further step to make a continuous synthesis-functionalization particle production line, a gas-phase functionalization method, as will be described below, is required.

Another challenge for particle functionalization is the characterization of surface layers. The chemical compositions of surface layers on functionalized nanoparticles can be studied using Fourier transform infrared spectroscopy (FTIR),[15,16] X-ray photoelectron spectroscopy (XPS),[13,17] or nuclear magnetic resonance (NMR).[12,13] Surface layer thicknesses are usually verified by transmission electronic microscopy (TEM). For organic monolayers on silicon particles, however, the thicknesses are close to the current resolution limit of TEM-based techniques. Moreover, monolayers are fragile to high-energy X-ray and electron beams. In this work, tandem differential mobility analysis (T-DMA)[18] is used to monitor monolayer formation online. The functionalization strategy could in principle be extended to any material system exhibiting appropriate mono-

(1) Herlin-Boime, N.; Jursikova, K.; Trave, E.; Borsella, E.; Guillois, O.; Fabbri, F.; Vicens, J.; Reynaud, C. *Mater. Res. Soc. Symp. Proc.* **2004**, *818*, 397.
(2) Lee, S.; Cho, W. J.; Han, I. K.; Choi, W. J.; Lee, J. I. *Phys. Status Solid B* **2004**, *241*, 2767.
(3) Dubertret, B.; Skourides, P.; Norris, D. J.; Noireaux, V.; Brivanlou, A. H.; Libchaber, A. *Science* **2002**, *298*, 1759.
(4) Bapat, A.; Anderson, C.; Perrey, C. R.; Carter, C. B.; Campbell, S. A.; Kortshagen, U. *Plasma Phys. Controlled Fusion* **2004**, *46*, B97.
(5) Raniero, L.; Zhang, S.; Aguas, H.; Ferreira, I.; Igreja, R.; Fortunato, E.; Martins, R. *Thin Solid Films* **2005**, *487*, 170.
(6) Canham, L. T. *Appl. Phys. Lett.* **1990**, *57*, 1046.
(7) Bley, R. A.; Kauzlarich, S. M. *J. Am. Chem. Soc.* **1996**, *118*, 12461.
(8) Li, X.; He, Y.; Talukdar, S. S.; Swihart, M. T. *Phase Transitions* **2004**, *77*, 131.
(9) Mangolini, L. T.; E.; Kortshagen, U. *Nano Lett.* **2005**, *5*, 655.
(10) Wolkin, M. V.; Jorne, J.; Fauchet, P. M.; Allan, G.; Delerue, C. *Phys. Rev. Lett.* **1999**, *82*, 197.
(11) Nayfeh, M. H.; Rogozhina, E. V.; Mitas, L. Synthesis, Functionalization and Surface Treatment of Nanoparticles **2003**, 173.
(12) Hua, F.; Swihart, M. T.; Ruckenstein, E. *Langmuir* **2005**, *21*, 6054.
(13) Zou, J.; Baldwin, R. K.; Pettigrew, K. A.; Kauzlarich, S. M. *Nano Lett.* **2004**, *4*, 1181.
(14) Taylor, B. R.; Fox, G. A.; Hope-Weeks, L. J.; Maxwell, R. S.; Kauzlarich, S. M.; Lee, H. W. H. *Mater. Sci. Eng., B* **2002**, *B96*, 90.
(15) Buriak, J. M. *Chem. Rev.* **2002**, *102*, 1271.
(16) Rogozhina, E.; Belomoin, G.; Smith, A.; Abuhassan, L.; Barry, N.; Akcakir, O.; Braun, P. V.; Nayfeh, M. H. *Appl. Phys. Lett.* **2001**, *78*, 3711.
(17) Legrand, J.; Taleb, A.; Gota, S.; Guittet, M. J.; Petit, C. *Langmuir* **2002**, *18*, 4131.
(18) Rader, D. J.; McMurry, P. H. *J. Aerosol Sci.* **1986**, *17*, 771.

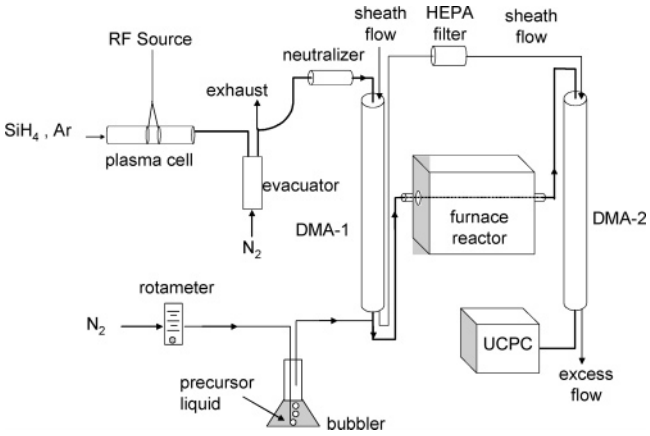

Figure 1. Schematic diagram of the experimental apparatus.

layer formation chemistry, especially for surface modification of particles that have been synthesized by gas-to-particle conversion.

In this paper, we describe a new functionalization method, in which organic monolayers are self-assembled onto the surfaces of aerosolized silicon nanoparticles continuously in gas phase. Crystalline silicon nanoparticles are produced by a nonthermal plasma method.[9] The particles are functionalized immediately after synthesis via the irreversible adsorption of amines, alkenes, alkynes, or aldehydes from the gas phase. The chemistries are analogous to some that have been reported for the functionalization of planar silicon surfaces.[15,16,19−22] This functionalization process provides a continuous production line for functionalized silicon nanoparticles, and the production lines can be parallelized to provide mass quantities.

Material and Methods

Experiments were conducted on crystalline silicon particles of 12.2 nm mobility diameter, using the atmospheric pressure aerosol flow tube reactor shown schematically in Figure 1. Silicon nanoparticles were synthesized from silane in a nonthermal, low-pressure (25 Torr) plasma reactor[9] and immediately extracted into the reactor using an air-operated vacuum pump (UV143H, AirVac Engineering, Seymour, CT). The carrier and sheath gases in the reactor were pure nitrogen. The polydisperse aerosol passed first through a bipolar diffusion charger and then through a differential mobility analyzer (DMA 3085, TSI Inc., Shoreview, MN) set to transmit positively charged particles of mobility diameter 12.2 nm. Precursors for the organic monolayers were added to the carrier gas stream immediately after mobility selection. Precursors were transported into the reaction zone by bubbling nitrogen at a known flow rate through a room-temperature vessel containing the precursor in its liquid state. The precursors investigated in this work included three amines, an alkene, an alkyne, and an aldehyde. Table 1 lists the precursors, all of which were obtained from Aldrich (Milwaukee, WI) and used without further purification. The combined particle/precursor/carrier gas streams were then passed through a heated reaction zone, which is where monolayer assembly occurred. The reaction zone consisted of a stainless steel tube surrounded by a tube furnace. The mean particle residence time in the reactor, τ, was varied by using tubes of different diameter, either 12 mm for $\tau \approx 1$ s or 25 mm for $\tau \approx 4$ s. The furnace setting, T_s, which corresponded to the maximum reactor temperature, could be adjusted between room temperature and 1100 °C. Adsorption onto the nanoparticles was monitored using tandem differential mobility analysis (T-DMA).[18] In T-DMA, a second DMA (DMA-2) is used in conjunction with an ultrafine condensation particle counter (UCPC 3025A, TSI Inc., Shoreview, MN) to determine the mobility diameters of particles in an aerosol stream.

Table 1. Monolayer Precursors Investigated, and Conditions for Formation of a saturated adlayer

precursor	T_s[a], °C	f_{N_2}[b], sccm	$\Delta\bar{D}_p$(max)[c], nm
tert-butylamine	250	76	0.6 ± 0.06
1-butylamine	275	64	1.4 ± 0.08
1-hexylamine	325	180	1.7 ± 0.10
1-hexene	500	350	1.5 ± 0.10
1-hexyne	300	64	1.6 ± 0.10
1-hexanal	325	340	1.4 ± 0.05

[a] Furnace setting temperature. [b] Nitrogen flow rate in precursor gas stream. [c] Compact monolayer thickness determined by TDMA.

Mobility selected particles were collected on a carbon TEM grid (Ted Pella Inc., Redding, CA) using an electrostatic sampler biased at −3.3 kV. Images were obtained using a Tecnai T12 microscope (FEI Company, Hilsboro, OR) operating at an accelerating voltage of 120 kV. Adsorbed layers were studied using diffuse reflectance Fourier transform infrared spectroscopy (DRIFTS). To collect enough particle samples for DRIFTS, the preclassification step was omitted (i.e., the particle streams bypassed DMA-1), and experiments were conducted under high flow rate conditions ($\tau \approx 0.1$ s). Samples were collected by inertial impaction onto stainless steel mesh filters for 90 min. Spectra of the collected particle samples were obtained at 2 cm^{-1} resolution with 32 scans using a Nicolet Magna-IR 750 spectrometer equipped with a diffuse reflectance accessory from Harrick Seagull.

Results and Discussion

Figure 2 shows representative transmission electron microscopy (TEM) images of mobility selected particles collected on a carbon TEM grid. The micrographs confirm that the particle stream after DMA-1 is monodisperse, and they establish that the particles are nearly spherical and of diameter ~12.2 nm. Particles are crystalline, as shown by the prominent 111 lattice fringes in the high magnification image in Figure 2c.[23,24]

Adsorption onto the nanoparticles was monitored using tandem differential mobility analysis (T-DMA).[18] Because adsorption onto a nanoparticle results in a size change, the difference in mobility diameter before and after adsorption can be used as a quantitative measure of uptake. Figure 3 shows a representative set of measurements. A stream of 12.2 nm mobility diameter particles was mixed with *tert*-butylamine [$(CH_3)_3CNH_2$], which was transported into the reaction zone at a carrier gas flow rate, f_{N_2}, of 76 standard $cm^3 \cdot s^{-1}$ (sccm). The mixture was passed the reactor at $T_s = 250$ °C and with $\tau = 1$

(19) Bent, S. F. *Surf. Sci.* **2002**, *500*, 879.
(20) Hamers, R. J.; Coulter, S. K.; Ellison, M. D.; Hovis, J. S.; Padowitz, D. F.; Schwartz, M. P.; Greenlief, C. M.; Russell, J. N., Jr. *Acc. Chem. Res.* **2000**, *33*, 617.
(21) Linford, M. R.; Chidsey, C. E. D. *J. Am. Chem. Soc.* **1993**, *115*, 12631.
(22) Wang, G. T.; Mui, C.; Musgrave, C. B.; Bent, S. F. *J. Am. Chem. Soc.* **2002**, *124*, 8990.
(23) Williams, D. B.; Carter, C. B. *Transmission Electron Microscopy: A Textbook for Materials Science*; Plenum Press: New York, 1996.
(24) Holmes, J. D. Z.; K. J.; Doty, R. C.; Pell, L. E.; Johnston, K. P.; Korgel, B. A. *J. Am. Chem. Soc.* **2001**, *123*, 3743.

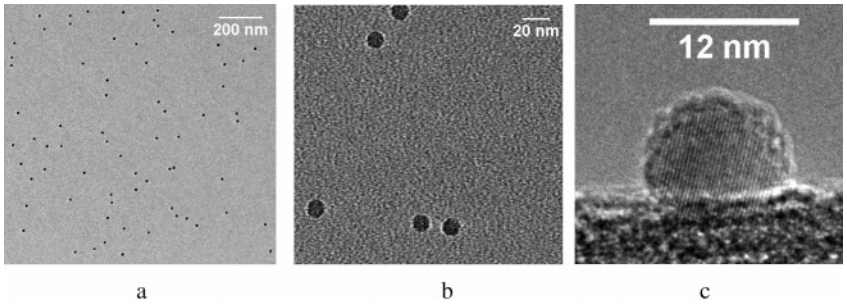

Figure 2. TEM images of particles collected after mobility classification by DMA-1 at 12.2 nm. (a) Plan-view image at low magnification, showing an ensemble of ~70 monodisperse particles. (b) A zoomed in region of the low magnification image, showing that particles are nearly spherical. (c) A high magnification, side-view image of one particle, showing a crystalline core surrounded by an amorphous shell. The lattice fringe spacing is 0.31 nm. The dark region in the lower part of the image is a lacey carbon support on the TEM grid.

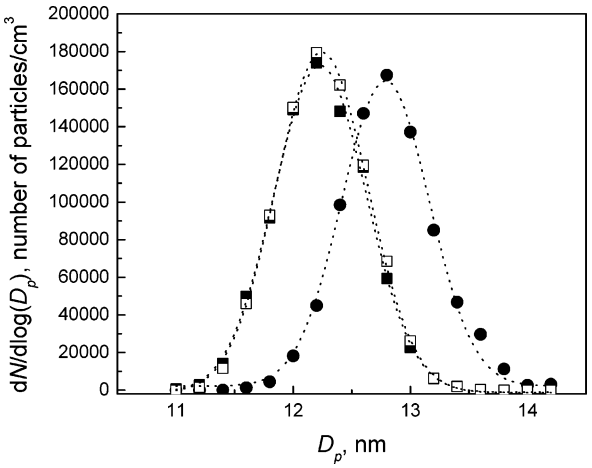

Figure 3. Representative T-DMA scans of 12.2 nm mobility selected particles with (●) and without (■, □) *tert*-butylamine exposure. The nitrogen carrier gas flow rate through the precursor vessel was 76 sccm, and the furnace setting was 250 °C. The dotted lines are best-fit Gaussian curves.

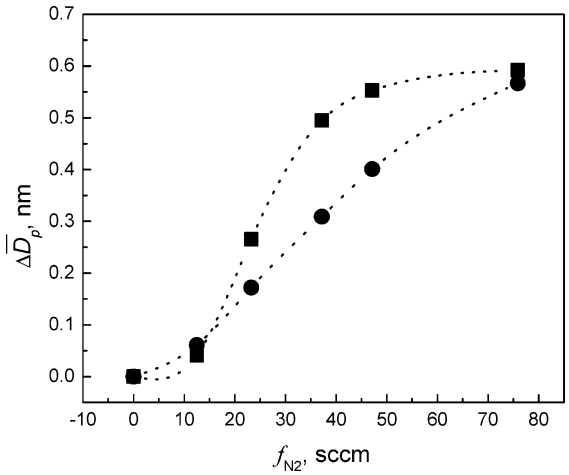

Figure 4. Change in peak mobility diameter ($\Delta\bar{D}_p$) plotted against the carrier gas flow rate in the *tert*-butylamine vessel (f_{N_2}). The furnace setting was 250 °C. Measurements are presented for two reaction residence times: $\tau = 1$ s (●) and $\tau = 4$ s (■).

s. Under these conditions, the T-DMA scans show that reaction with *tert*-butylamine results in an increase in peak particle mobility diameter, $\Delta\bar{D}_p$, of 0.6 nm. Control experiments were conducted, in which only *tert*-butylamine and nitrogen, but no particles, were passed through the reactor. No particles were detected, which establishes that the change in the peak particle mobility diameter is due to a modification of the original particle stream, not to the appearance of new particles from *tert*-butylamine decomposition.

The differential mobility analyzers used for this work are exceptionally stable, and measured distributions are virtually unchanged from day to day. Figure 3 shows the results of two control experiments conducted roughly 1 h apart. Two T-DMA scans were recorded after passing a 12.2 nm mobility selected particle stream through the reactor but without *tert*-butylamine present. The peak mobility diameters in both scans are at 12.2 nm, and the scans are virtually superimposable. Because of the stability of our instrument, we believe that we can measure changes in particle mobility diameter at least as small as 0.1 nm.[25−27]

Figure 4 plots $\Delta\bar{D}_p$, the change in peak mobility diameter, vs f_{N_2} through the *tert*-butylamine bubbler at a furnace setting of 250 °C. Under the conditions of these experiments, f_{N_2} is approximately proportional to the *tert*-butylamine partial pressure. Measurements are presented for two residence times, $\tau =$ 1 and 4 s. The measured peak mobility diameters increase with f_{N_2} at low flow rates, and uptake increases more rapidly with f_{N_2} at $\tau = 4$ s than it does at $\tau = 1$ s. Both of these observations are consistent with collision-limited uptake kinetics in the low uptake regime. At high flow rates, however, both plots converge to the same maximum $\Delta\bar{D}_p$ value of 0.6 nm. That $\Delta\bar{D}_p$ saturates and that the maximum value of $\Delta\bar{D}_p$ is independent of reactor residence time clearly indicates that the silicon particles become saturated with *tert*-butylamine. The maximum diameter change implies a layer ~0.3 nm thick, which is roughly equal to the length of the N−C−C chain in *tert*-butylamine.

The interaction of 1-butylamine with 12.2 nm silicon particles at different furnace setting temperatures was also studied. Figure 5 shows how $\Delta\bar{D}_p$ varies with f_{N_2} for 1-butylamine adsorption at furnace settings of 200, 225, 250, and 275 °C. All results were obtained under conditions of $\tau \approx 4$ s. (Because of gas expansion effects in the heated reaction zone, τ is weakly dependent on the furnace setting.) For all furnace settings studied, $\Delta\bar{D}_p$ increases with the carrier gas flow rate f_{N_2}, and the slope increases more rapidly at a higher furnace setting, indicating that precursors is chemically absorbed onto silicon nanoparticles. At the lowest furnace temperatures studied, $\Delta\bar{D}_p$ does not saturate, but at 250 and 275 °C, a saturation value is reached, at $\Delta\bar{D}_p = 1.4$ nm. As was the case for *tert*-butylamine,

(25) Higgins, K. J.; Jung, H.; Kittelson, D. B.; Roberts, J. T.; Zachariah, M. R. *J. Phys. Chem.* **2002**, *106*, 96.
(26) Higgins, K. J.; Jung, H.; Kittelson, D. B.; Roberts, J. T.; Zachariah, M. R. *Environ. Sci. Technol.* **2003**, *37*, 1949.
(27) Nienow, A. M.; Roberts, J. T.; Zachariah, M. R. *J. Phys. Chem. B* **2005**, *109*, 5561.

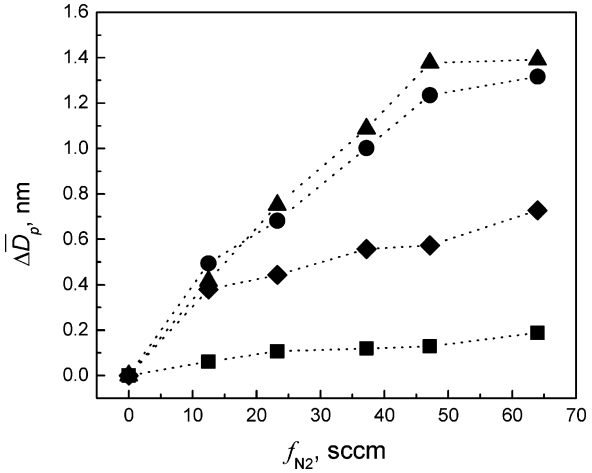

Figure 5. Change in peak mobility diameter ($\Delta\bar{D}_p$) plotted against the carrier gas flow rate in the 1-butylamine vessel (f_{N_2}). The furnace settings were 200 °C (■), 225 °C (●), 250 °C (◆), and 275 °C (▲).

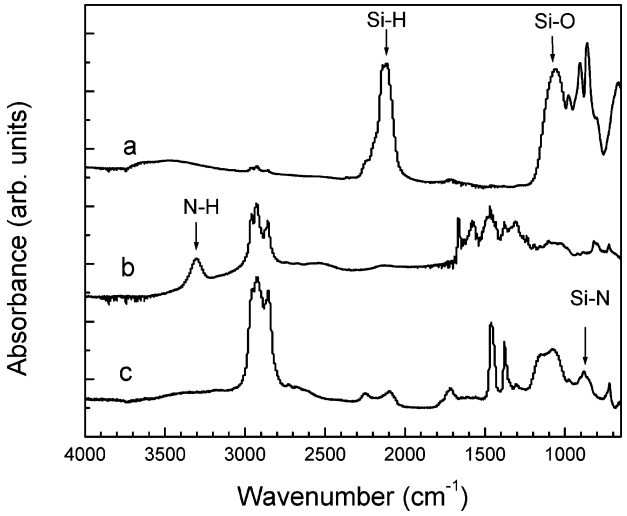

Figure 6. Diffuse reflectance Fourier transform infrared spectra of (a) uncoated silicon nanoparticles, (b) neat 1-hexylamine, and (c) silicon nanoparticles coated with 1-hexylamine. Sample preparation is described in the text.

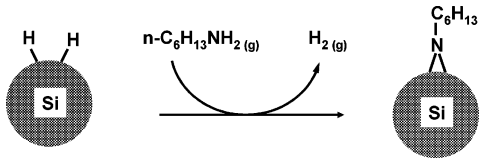

Figure 7. Proposed scheme for irreversible 1-hexylamine adsorption by a hydrogenated silicon nanoparticle.

the saturation value is approximately equal to twice the length of the adsorbing hydrocarbon chain.

Silicon nanoparticles readily take up, in addition to *tert*-butylamine and 1-butylamine, 1-hexylamine, and they also adsorb alkenes, alkynes, and aldehydes. In all cases, uptake reaches a maximum value of $\Delta\bar{D}_p$ that is suggestive of an adsorbed monolayer. The average values and uncertainties of maximum $\Delta\bar{D}_p$ obtained from at least three TDMA scans are summarized in Table 1. For the amines, which presumably are anchored to silicon through the same type of bond, $\Delta\bar{D}_p$(max) depends strongly on the alkyl chain length: 0.6 nm for *tert*-butylamine, 1.4 nm for 1-butylamine, and 1.7 nm for 1-hexylamine. For adsorbates that contain a C_6 chain (1-hexylamine, 1-hexene, 1-hexyne, and 1-hexanal), $\Delta\bar{D}_p$(max) is always close to 1.5 nm. Assuming that adsorption is isotropic, $\Delta\bar{D}_p$(max) must be twice the thickness of the adsorbed layer. In all cases, the layer thickness is roughly the length of the adsorbed hydrocarbon chain.

Figures 6 shows two representative spectra of the silicon particles, one of untreated particles and one of particles exposed to 1-hexylamine; the furnace setting in both cases was 325 °C. Figure 6 also shows a spectrum of neat 1-hexylamine, the sample of which was prepared by dropping about ~1 mL of liquid directly onto a piece of mesh. The most prominent band in FTIR spectra of uncoated particles (Figure 6a) is at ~2150 cm^{-1}. It is attributed to ν(Si−H);[11] because particles are generated in a hydrogen-rich environment, they presumably leave the plasma reactor with a saturated hydrogen adlayer. Spectra of untreated particles also show a broad peak near 1100 cm^{-1}. This is assigned to oxidized Si[11] that forms when samples are transported in air from the aerosol flow reactor to the spectrometer. The coated particle spectra (Figure 6c) show clear evidence of an organic adlayer: a broad C−H stretching band in the 2900−3000 cm^{-1} region, hydrocarbon skeletal bands at 1377 and 1460 cm^{-1}, and a feature at 860 cm^{-1} that we assign to the Si−N bond.[11,16] Although the skeletal region in the coated particle spectra is simpler than that in the condensed 1-hexylamine spectra, the asymmetric CH_2 stretching located at 2923 cm^{-1} in the IR spectra indicates that the hydrocarbon chain possesses a spatial arrangement between the all-trans (2916 cm^{-1}) and all-gauche (2926 cm^{-1}) position. This is possibly because the particle surface curvature allows certain degree of free molecule motion in the monolayer. It is also noteworthy that ν(Si−H) is virtually absent in the coated particle spectra and that there is almost no intensity in the N−H stretching region (~3300 cm^{-1}, see Figure 6b). Taken together, these observations imply that 1-hexylamine adsorbs on a silicon nanoparticle to form a compact monolayer, and that the attachment chemistry involves hydrosilylation chemistry. Figure 7 shows schematically how 1-hexylamine adsorption might occur.

Because of the high flow rate conditions that were used to collect samples for FTIR analysis, the residence time in the reactor was quite short (~0.1 s), and formation of a saturated adsorbed layer may not have occurred. This may explain the appearance of a broad peak near 1100 cm^{-1}, attributed to oxidized silicon, in the coated particle spectra. The absorbance of the Si−O peak, however, is much smaller than that of the uncoated particles, generally twice as much after 1 h exposure. Moreover, after seven months exposure to the air, the IR spectra of the coated particle remain the same features except with a 60% higher Si−O absorbance, indicating that the hydrocarbon is attached to the silicon surface stably and the adsorbed layer significantly slows oxidation. Additional work is underway to determine the extent to which coated particles are protected against oxidation.

Conclusions

This study provides the first example of monolayer assembly onto aerosolized silicon nanoparticles via adsorption from the gas phase. Crystalline silicon nanoparticles were extracted from a nonthermal plasma. Preselected monodisperse particles of 12.2 nm diameter were functionalized with amines, alkenes, alkynes, and aldehydes via thermal activation in a furnace tube reactor at temperature of 250−500 °C with a residence time of less

than 4 s. The changes in particle size $\bar{D}_p$ after the reactions are directly detected online by tandem differential mobility analysis. $\Delta\bar{D}_p$ increases with increasing organic vapor pressure until the formation of a saturate monolayer. The rate of hydrosilylation reaction also rises with increasing residence time and furnace setting temperature, indicating the organic molecules are chemically adsorbed onto the silicon nanoparticle surfaces. The functionalized particles are further characterized with FTIR to obtain the bonding information between the organic molecules and silicon nanoparticle surface. The approach is in principle generalizable, and it could be extended to any aerosol system for which appropriate functionalization schemes are available. Moreover, aerosol-state modification is scalable and could be used to generate gram-quantities (or greater) of material. For these reasons, the method described in this paper has great promise.

Acknowledgment. This work was supported in part by the National Science Foundation under Grant No. 0094911 and in part by the MRSEC Program of the National Science Foundation under Award DMR-0212302. The authors thank U. Kortshagen and L. Mangolini for their assistance in silicon nanoparticle generation.

JA0611238